



Pa² kinematic bond in translational parallel manipulators

Alfonso Hernández¹, Erik Macho¹, Mónica Urizar¹, Víctor Petuya¹, and Zhen Zhang²

¹Department of Mechanical Engineering, University of the Basque Country (UPV/EHU), Bilbao, Spain

²Mechanical Engineering College, Tianjin University of Science and Technology, Tianjin, China

Correspondence: Victor Petuya (victor.petuya@ehu.es)

Received: 16 May 2017 – Revised: 2 November 2017 – Accepted: 18 December 2017 – Published: 22 January 2018

Abstract. The Pa² pair is composed of two intertwined articulated parallelograms connecting in parallel two links of a kinematic chain. This pair has two translational degrees of freedom leading to a translational plane variable with the position. Currently, the Pa² pair appears in conceptual designs presented in recent papers. However, its practical application is very limited. One of the reasons for this can be the high number of redundant constraints it has. But, it has to be considered that most of them can be eliminated by replacing wisely the revolute joints by spherical joints. On the other side, the structure of the Pa² pair contributes to increase the global stiffness of the kinematic chain in which it is mounted. Also, its implementation is a promising alternative to the problematic passive prismatic joints. In this paper, the Pa² pairs are used in the design of a 3-PPa² parallel manipulator. The potentiality of this design is evaluated and proven after doing the following analyses: direct and inverse kinematics, singularity study, and workspace computation and assessment.

1 Introduction

In the field of structural analysis of mechanisms, it is very common to work with R (revolute) joints, P (prismatic) joints, C (cylindrical) joints, etc. which are mechanical connections between adjacent elements permitting some degrees of freedom in their relative motion. Nevertheless, the idea of kinematic joint or pair has always been a more general concept than a simple mechanical coupling (Angeles, 2005). As an example, we can think about the U (universal) joint, in which the pair itself contains an intermediate moving element, the cross shaft. This is the idea that underlies the kinematic joint named Pa joint (also known as Π joint; Hervé and Sparacino, 1992), and other more complex pairs, that can be included in a further generalized concept first termed by Hervé (1999) as liaison cinématique in French or mechanical bond in English. Later on, Yu et al. (2009) renamed this type of pairs, those that can be even formed by closed-loop kinematic chains, as complex joints (CJs), group in which the Pa joint is included. In Yu et al. (2009), the authors present an in-depth state of the art of these CJs and propose a new type classification and mobility analysis for these special joints.

Regarding the Pa joint, it consists of an articulated parallelogram which permits a translational degree of freedom (dof), and it is commonly used in the design of translational parallel manipulators (Gogú, 2004). One of the first practical application of the Pa joint was in the Delta translational manipulator (Clavel, 1988) designed by Raymond Clavel for Pick & Place operations. A similar architecture was the STAR parallel manipulator, proposed by Hervé and Sparacino (1992) in which this special kinematic pair was named as Π joint. The CAPAMAN robot designed by Ceccarelli and Ottaviano (2000) at the Laboratory of Robotics and Mechatronics (Cassino) is also another practical example of a three dof spatial parallel manipulator which incorporates an articulated parallelogram in each leg. A 2-D version of the Delta robot, named the Diamond robot, which also incorporated parallelogram linkages, was designed by Huang et al. (2004) for quality inspection of rechargeable batteries. The robot named Par4 (Pierrot et al., 2009), which is an enhanced design of the prior H4 (Pierrot and Company, 1999), incorporates the Pa joint not only in the legs of the manipulator but also in the special moving platform the authors termed as the traveling plate, allowing for a rotational dof in the end-effector without the need of a telescopic chain as occurs in the Delta design. Another robot with pure translational mo-

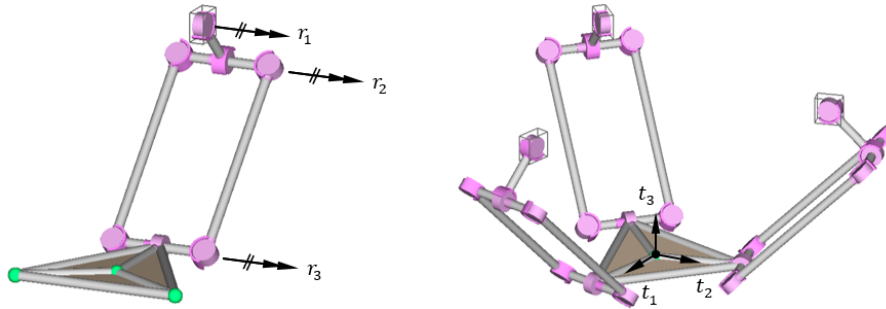


Figure 1. Delta Robot (three translations t_1 , t_2 and t_3).

tion incorporating the Pa joint is the Micro Finger (Arai et al., 1996), a 3 dof parallel platform intended for manipulating micrometer size objects.

We can find in the scientific literature more architectures formed by the Pa joint, such as the two Schönflies designs, the 4 – RRPaR and 4 – PRPaR, proposed recently by Li et al. (2013) or the translational parallel manipulator presented by Affi et al. (2004), formed by three prismatic legs and two Pa joint based passive chains that eliminate the rotational capacity of the manipulator. However, it is quite notable the limited use of double Pa joints, termed as the Pa² joint. The kinematic Pa² joint is composed of two intertwined articulated parallelograms which connect in parallel the two elements that the joint links together. It possesses two translational dof that result in a translational plane varying with the position. A design with a double Pa joint, named by the author as the Π^2 joint, was proposed by Angeles (2004). In the proposed design, the Π^2 joint consist of four in-parallel bars connecting the fixed and moving platform with universal joints. This joint permits two translational dof, where the moving platform traces a spherical translational motion with respect to the fixed platform. Their kinematic characteristics are equivalent to those of the Pa² joint.

The first clear proposal of designs including Pa² joints is found in the Doctoral Thesis of Oscar Salgado (2008), where two 4 dof parallel manipulators based on Pa² joints are investigated by means of Theory of Group of Displacements. Both robots are formed by four kinematic chains, each one generating 5 dof, the connection of all kinematic chains resulting in a Schönflies motion (3 translations and 1 rotation) in the moving platform. Some works related to this Thesis can be found in Salgado et al. (2007) where a parallelogram-based 4 dof manipulator intended for aeronautical industry is presented, and in Salgado et al. (2008) in which a new topology of 3T1R fully-parallel manipulator intended for Pick and Place operations is proposed.

With the purpose of evaluating the potential of a certain design of a parallel manipulator including this type of Pa joints, one of the main steps is to assess the operational workspace the manipulator can reach. This study is included in the last part of the present paper. As proposed in Macho

et al. (2008, 2013), a complete analysis of the workspace requires the study of the singularity locus, as well as the determination of the working modes and the singularity-free regions associated with each working mode, so that an enlarged workspace can be found. A general systematic procedure to obtain all the singularity-free workspace regions in parallel manipulators, so that strategies to enlarge the accessible workspace can be planned, is presented in Macho et al. (2009).

The outline of the paper is the following. Firstly, a detailed description of the kinematic characteristics and current usage of the Pa joint will be introduced, and, based on that, the double Pa joint, that is, the Pa² joint, will be described. Next, a complete kinematic analysis of a new manipulator designed using Pa² joints will be presented, the 3 – PPa² parallel manipulator. This study includes the mobility analysis, the solution of the direct and inverse position problems, the solution of the velocity problem, the singularity analysis and the workspace computation. Finally, the main conclusions will be presented.

2 The Pa² kinematic bond in translational parallel manipulators

The Pa joint is based on a planar four-bar linkage in a parallel configuration (or articulated parallelogram). As it is known, the four-bar linkage is a one degree of freedom mechanism and in a general configuration, the coupler element has an instantaneous rotation. However, in a parallel configuration, its instantaneous center of velocity goes to infinity. In this case, the coupler element moves following a permanent circumferential translation.

This is called the Pa joint, which has been successfully used in some translational parallel manipulators. Maybe, as pointed out in the introduction, the best-known example is the Delta robot, shown in Fig. 1, which is built from 3 – RRPaR kinematic chains joining in a parallel architecture the fixed frame and the moving platform. The RRPaR kinematic chain has four degrees of freedom, three translations and one rotation, that is, it is a Schönflies motion generator. One translation comes from the Pa joint, while the remaining

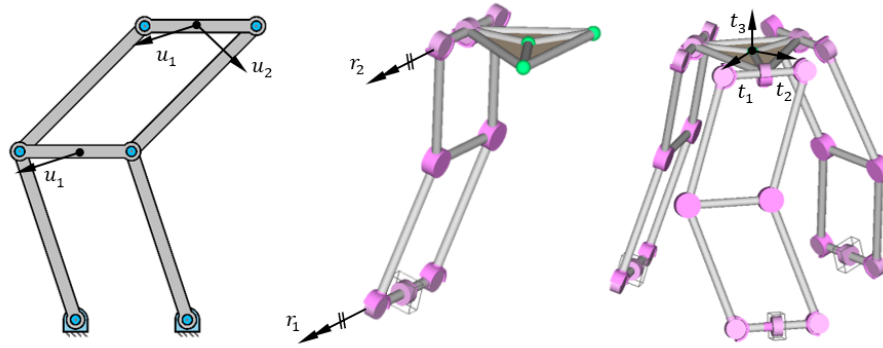


Figure 2. Micro Finger manipulator (three translations t_1 , t_2 and t_3).

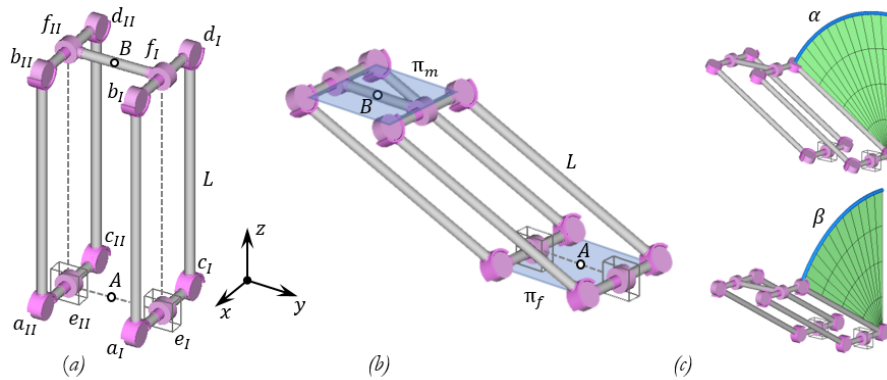


Figure 3. Pa² joint. Modelization and associated motion.

three parallel rotation axes (r_1 , r_2 , r_3 in Fig. 1) provide the final rotation and the other two translations.

One of the main principles of the structural synthesis is the fact that in a parallel manipulator the mobility of the moving platform is the intersection of mobilities of the kinematic chains. This is the reason why in the Delta robot the rotational degree of freedom is lost. Each chain allows just a rotation around the direction of its parallel revolute joints. Since such a direction is not the same in the three chains, no rotation of the moving platform is possible when all chains are assembled.

More than one Pa joint can be combined in the same chain. As an example, the Micro Finger parallel manipulator, shown in Fig. 2, is built from three chains containing each one two Pa joints serially connected. This configuration provides at each chain two translational degrees of freedom (u_1 , u_2), that is, a plane of translations. The kinematic chains of this example contain these double Pa joints and two parallel revolute joints (r_1 , r_2), which provide the third translation and an extra rotational degree of freedom which is lost when all chains are assembled in parallel.

Finally, several Pa joints can be connected in order to build the Pa² joint, which will be used in the translational manipulator of this work. As it can be seen in Fig. 3a, it is con-

stituted by two identical Pa joints ($a_I b_I c_I d_I$ and $a_{II} b_{II} c_{II} d_{II}$), which are parallel one to the other, and there is also a third Pa in a crossed orientation, $e_I f_I e_{II} f_{II}$, connecting the previous ones. The axes of the revolute joints in the two parallel Pa have the same direction, while the axes in the cross-linked Pa are perpendicular to the previous ones. This assembly has 2 dof and 8 redundant constraints.

Taking into account the geometry of the resulting architecture, two imaginary planes appear, the fixed plane π_f and the coupler plane π_m , which are always parallel, Fig. 3b. This means that the two dof are translational, like in the previously shown double Pa, but in this case, instead of being planar, this translation is spherical. The two parallel Pa rotate an angle α and the crossed Pa rotates angle β , Fig. 3c. The equation relating the coordinates of reference points A and B is:

$$(x_B - x_A)^2 + (y_B - y_A)^2 + (z_B - z_A)^2 = L^2 \quad (1)$$

Or alternatively, given a reference system as shown in the figure:

$$\begin{aligned} x_B - x_A &= L \sin \beta \\ y_B - y_A &= -L \cos \beta \sin \alpha \\ z_B - z_A &= L \cos \beta \cos \alpha \end{aligned} \quad (2)$$

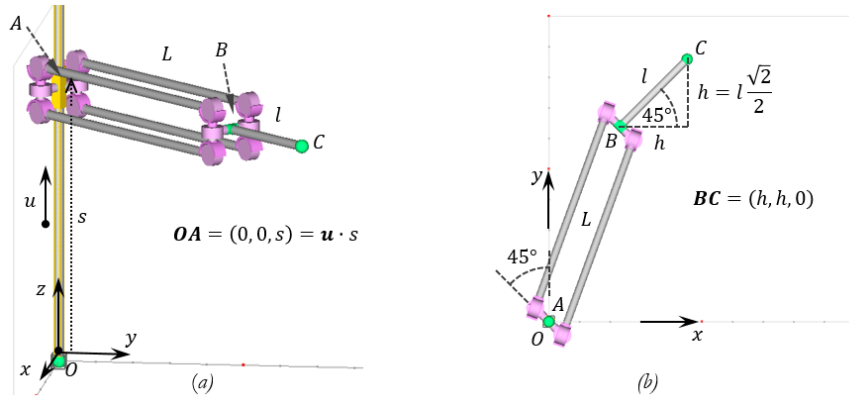


Figure 4. PPa² kinematic chain.

Next, the mobility analysis of two translational parallel manipulators proposed by the authors which include the Pa² kinematic joint will be developed.

2.1 Mobility analysis in 3 – PPa² and 3 – CP²R Parallel Manipulators

2.1.1 3 – PPa² translational parallel manipulator

The PPa² kinematic chain generates a translational motion in space. Indeed, its corresponding kinematic bond is the product of two translational kinematic bonds: one of dimension 1, {T_u}, and another of dimension 2, {T_{v,w}}, where u, v and w are three linearly independent vectors which represent their associated translational directions.

The resulting D_e displacement is the product of both bonds:

$$D_e = \{T_u\} \cdot \{T_{v,w}\} = \{T_3\} \quad (3)$$

Therefore, the displacement achieved in the end-effector of the PPa² chain belongs to the subgroup {T₃} of translations in space.

By linking three identical kinematic chains to a moving platform we get a displacement of this moving platform. This displacement or motion pattern results from intersecting the displacements associated with each chain. That is:

$$D_e = \bigcap_{i=1}^3 \{T_3\}_i = \{T_3\} \quad (4)$$

This yields again a translational displacement of dimension 3.

2.1.2 3 – CPa²R translational parallel manipulator

The kinematic bond of the CPa²R kinematic chain is the product of three kinematic bonds. The one corresponding to the cylindrical pair is a kinematic bond of dimension 2, {C_A}, which includes a rotation around an A axis and a translation

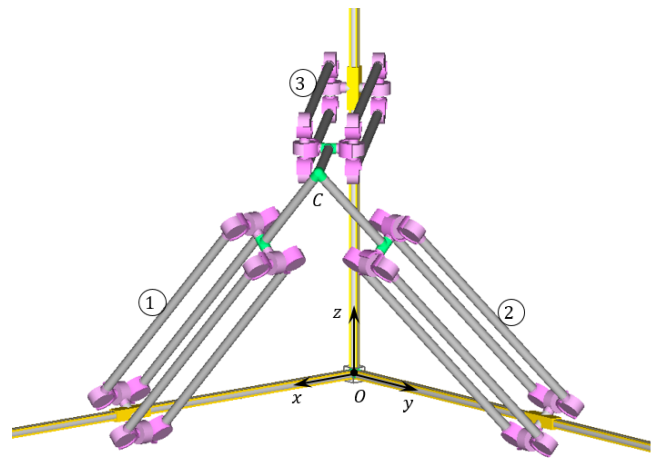


Figure 5. 3 – PPa² parallel manipulator.

in the direction of that axis. The one corresponding to the Pa² pair, {T_{v,w}}, has been previously described; and the rotation of the last revolute pair is a bond of dimension 1, {R_B}, which includes a rotation around a B axis.

Hence, the resulting D_e displacement is the product of three bonds:

$$D_e = \{C_A\} \cdot \{T_{v,w}\} \cdot \{R_B\} = \{T_3\} \cdot \{R_A\} \cdot \{R_B\} \quad (5)$$

Under the assumption that the translational directions are independent one from another and, additionally, the rotational ones, then the displacement generated in the end-effector of the CPa²R chain has dimension 5, 3T2R three translations and two rotations. These displacements constitute a subset of solid element displacements of dimension 6, {D_e}. However, it does not have group structure.

As before, by linking three identical kinematic chains to a moving platform a displacement of this moving platform is achieved. This displacement or motion pattern results from intersecting the displacements associated with each chain.

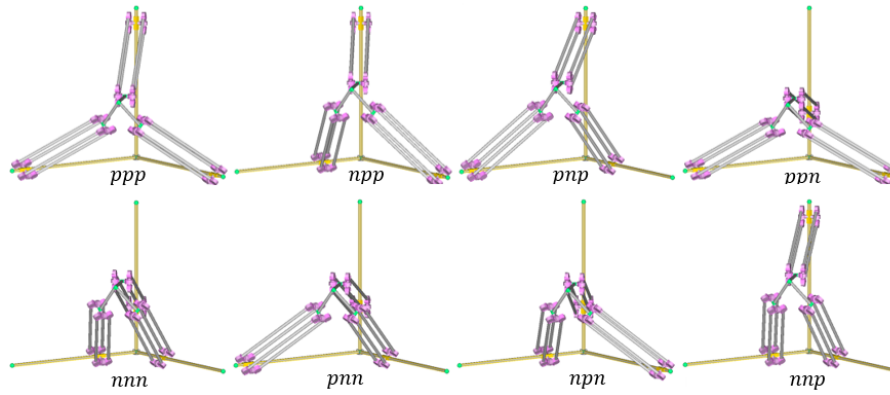


Figure 6. The eight existing working modes.

That is:

$$D_e = \bigcap_{i=1}^3 (\{T_3\} \cdot \{R_A\} \cdot \{R_B\})_i = \{T_3\} \quad (6)$$

This yields again a translational displacement of dimension 3. This happens because the planes that contain the rotational directions of each leg intersect at one point, so that there is no rotational direction common to the three legs of the manipulator. On the contrary, the three translations of the legs are common to all of them and, thus, they remain in the motion of the moving platform.

In comparison to the previous manipulator, this design has six redundancies less than the first one. As both manipulators have the same kinematics and knowing that the 3-PPa² is composed of a less number of joints, the constructive design is simpler in the 3-PPa² translational parallel manipulator, which is the one that will be subsequently analyzed.

3 The 3-PPa² parallel manipulator

In references Hernandez et al. (2016a, b), a preliminary kinematic analysis of the manipulator under study was presented, showing the potential this manipulator has. As it will be shown in this section and subsequent ones, we present here a reformulated kinematic analysis based on an equivalent simplified manipulator. From this new formulation, a complete workspace and joint-space analysis is accomplished by means of obtaining the set of working modes and assembly modes, the singularity-free regions associated with each of the assembly modes and the enlarged operational workspace.

In the proposed 3-PPa² manipulator, shown in Fig. 4, one translation is provided by the prismatic P joint and the remaining two ones by the Pa² joint. The slider goes along the direction of one Cartesian axis of the global reference frame and the home position of the Pa² is set as the pose having all links perpendicular among them, as it is shown in Figs. 3a and in 4a. The BC link of the moving platform is normal to the coupler plane of the Pa². The dimensional

parameters are just the lengths L and l . The coordinates of point C are the output variables, while the distance s from the prismatic slider to the origin is the input variable. The closure loop equation relating all parameters can be obtained in a very simple way particularizing Eq. (1) for this case. Considering a vertical leg, as shown Fig. 4b:

$$\begin{aligned} ((x_C - h) - 0)^2 + ((y_C - h) - 0)^2 + ((z_C - 0) - s)^2 &= L^2 \\ (x_C - h)^2 + (y_C - h)^2 + (z_C - s)^2 &= L^2 \end{aligned} \quad (7)$$

As it can be seen in Fig. 5, it has been chosen a configuration for the manipulator based on three identical chains with the P sliders along the three Cartesian axes of the global reference system (the three sliding directions intersecting at the origin O).

To solve any kinematic problem, the first step is to pose the position equations system of the assembled manipulator:

$$\begin{cases} ec_1 = (x_C - s_1)^2 + (y_C - h)^2 + (z_C - h)^2 - L^2 = 0 \\ ec_2 = (x_C - h)^2 + (y_C - s_2)^2 + (z_C - h)^2 - L^2 = 0 \\ ec_3 = (x_C - h)^2 + (y_C - h)^2 + (z_C - s_3)^2 - L^2 = 0 \end{cases} \quad (8)$$

4 Position problem

The system of closure loop equations of the three chains contains the input and output variables and is used to solve the position problem.

The different solutions of the inverse position problem, which are also called working modes of the manipulator, are found in an easy way because they are decoupled. Given the coordinates of the coupler point C , each chain can have independently two different positions, or values of its input variable.

$$\begin{cases} s_1 = x_C \pm \sqrt{(y_C - h)^2 + (z_C - h)^2 - L^2} \\ s_2 = y_C \pm \sqrt{(x_C - h)^2 + (z_C - h)^2 - L^2} \\ s_3 = z_C \pm \sqrt{(x_C - h)^2 + (y_C - h)^2 - L^2} \end{cases} \quad (9)$$

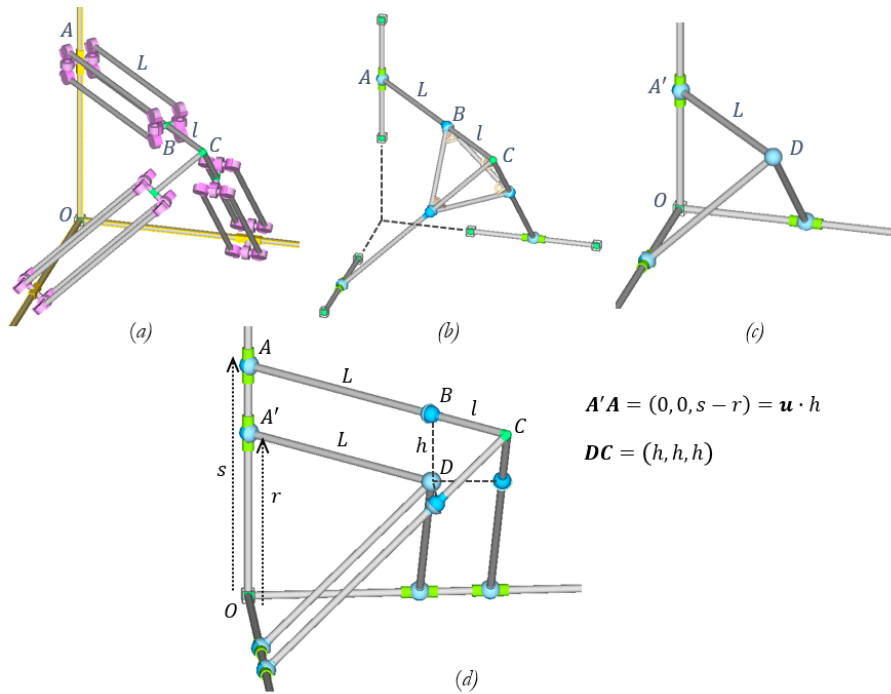


Figure 7. Equivalent simplified manipulator.

Combining these two solutions for the three chains the manipulator presents a total of eight working modes. In Fig. 6, p and n denote the positive or negative sign of the square root involved in Eq. (9).

On the contrary, the direct position problem is not so decoupled. To solve this problem, some algebraic manipulation on this Eq. (8) is required, to eliminate, for example, the output variables y_C and z_C , and achieve the univariate polynomial in the output variable x_C . A quadratic polynomial is obtained, whose coefficients depend on the input variables, s_1, s_2 and s_3 :

$$ax_C^2 - (2ah + c_1)x_C + ah^2 + c_1h + (s_1 - h)^2b_1 + ((s_2 - h)^2 + (s_3 - h)^2 - 4L^2)a_{23}^2 = 0 \quad (10)$$

Where:

$$\begin{aligned} a_{12} &= (s_1 - h)(s_2 - h) & a_{23} &= (s_2 - h)(s_3 - h) \\ a_{31} &= (s_3 - h)(s_1 - h) \\ b_1 &= a_{12}^2 + a_{31}^2 & b_2 &= a_{23}^2 + a_{12}^2 \\ b_3 &= a_{31}^2 + a_{23}^2 \\ a &= 2(b_1 + b_2 + b_3) = 4(a_{12}^2 + a_{23}^2 + a_{31}^2) \\ c_1 &= 4(s_1 - h)b_1 \end{aligned} \quad (11)$$

In this process, the values of the output coordinates y_C and z_C as functions of inputs and x_C are also obtained. Once x_C is obtained, the remaining output variables yield:

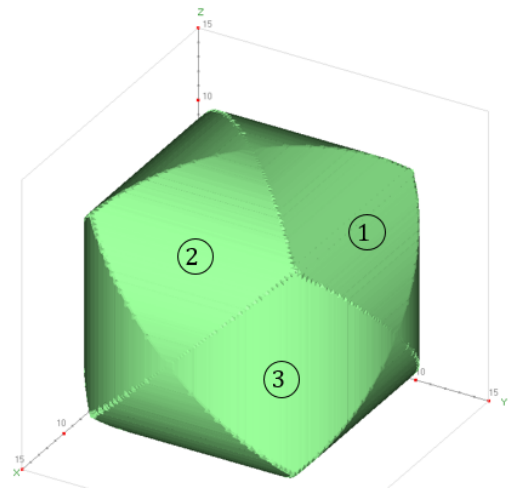
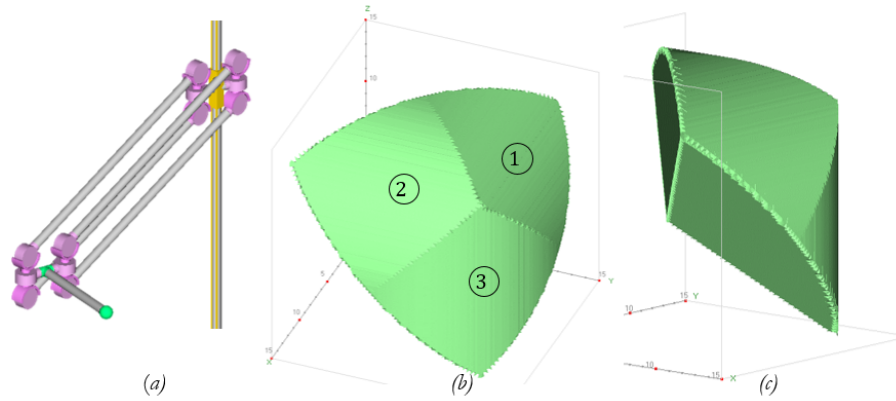


Figure 8. Theoretical workspace.

$$\begin{aligned} y_C &= h + \frac{(s_2 - h)^2 - (s_1 - h)^2 + 2(s_1 - h)x_C}{2(s_2 - h)} \\ z_C &= h + \frac{(s_3 - h)^2 - (s_1 - h)^2 + 2(s_1 - h)x_C}{2(s_3 - h)} \end{aligned} \quad (12)$$

Obviously, for given values of the inputs there are two solutions of the direct problem, also called assembly modes. The final solutions of the direct position problem are:


Figure 9. Real workspace.

$$\begin{aligned}
 x_C &= h + \frac{(s_1 - h)b_1 \pm a_{23}\sqrt{\Delta_s}}{a/2} \\
 y_C &= h + \frac{(s_2 - h)b_2 \pm a_{31}\sqrt{\Delta_s}}{a/2} \\
 z_C &= h + \frac{(s_3 - h)b_3 \pm a_{12}\sqrt{\Delta_s}}{a/2}
 \end{aligned} \quad (13)$$

Being:

$$\begin{aligned}
 \Delta_s &= (s_1 - h)^2 b_1 + (s_2 - h)^2 b_2 + (s_3 - h)^2 b_3 \\
 &\quad + 2(s_1 - h)^2 (s_2 - h)^2 (s_3 - h)^2 - L^2 a
 \end{aligned} \quad (14)$$

Kinematic problems can be solved in an easier way making use of a simplified equivalent manipulator, shown in Fig. 7. To understand better the transformation, first an intermediate schematic representation is done, Fig. 7b, where each Pa² joint is depicted as a single bar of the same length L with spherical joints. Next, the moving platform is merged into a single point D , making null the length l , resulting in the 3- \underline{PSS} parallel manipulator, Fig. 7c. This process implies that each bar AB is translated to its new equivalent position $A'D$ a magnitude h along the direction of its slider, as shown in Fig. 7d.

Since the directions of bars of the 3- \underline{PPa}^2 manipulator and those of the 3- \underline{PSS} are always parallel, from a kinematic point of view both are fully equivalent, this is, both have the same solutions and singularities. The relations between the input and output variables of the real and the simplified manipulator are:

$$\begin{aligned}
 s_i &= r_i + h, \quad i = 1, 2, 3 \quad x_C = x_D + h, \\
 y_C &= y_D + h, \quad z_C = z_D + h
 \end{aligned} \quad (15)$$

Then, for example, for the kinematic chain with vertical sliding direction:

$$\begin{aligned}
 &((x_D + h) - h) + ((y_D + h) - h)^2 \\
 &\quad + ((z_D + h) - (r_3 + h))^2 = L^2 \\
 x_D^2 + y_D^2 + (z_D - r_3)^2 &= L^2
 \end{aligned} \quad (16)$$

Using the equivalent manipulator, the solutions of the direct position problem are obtained from:

$$\begin{cases}
 (x_D - r_1)^2 + y_D^2 + z_D^2 = L^2 \\
 x_D^2 + (y_D - r_2)^2 + z_D^2 = L^2 \\
 x_D^2 + y_D^2 + (z_D - r_3)^2 = L^2
 \end{cases} \quad (17)$$

Then, the quadratic univariate polynomial in x_D and the values of y_D and z_D are:

$$\begin{aligned}
 &(r_1^2 r_2^2 + r_2^2 r_3^2 + r_3^2 r_1^2)(2x_D)^2 - 2r_1^3 (r_2^2 + r_3^2) 2x_D \\
 &\quad + r_1^4 (r_2^2 + r_3^2) + (r_2^2 + r_3^2 - 4L^2) r_2^2 r_3^2 = 0
 \end{aligned} \quad (18)$$

$$2y_D = \frac{r_2^2 - r_1^2 + r_1 2x_D}{r_2} \quad 2z_D = \frac{r_3^2 - r_1^2 + r_1 2x_D}{r_3} \quad (19)$$

And finally:

$$\begin{aligned}
 2x_D &= \frac{r_1^2 (r_2^2 + r_3^2) \pm r_2 r_3 \sqrt{\Delta_r}}{r_1^2 r_2^2 + r_2^2 r_3^2 + r_3^2 r_1^2} \\
 2y_D &= \frac{r_2^3 (r_3^2 + r_1^2) \pm r_3 3r_1 \sqrt{\Delta_r}}{r_1^2 r_2^2 + r_2^2 r_3^2 + r_3^2 r_1^2} \\
 2z_D &= \frac{r_3^3 (r_1^2 + r_2^2) \pm r_1 r_2 \sqrt{\Delta_r}}{r_1^2 r_2^2 + r_2^2 r_3^2 + r_3^2 r_1^2}
 \end{aligned} \quad (20)$$

Where:

$$\begin{aligned}
 \Delta_r &= r_1^4 (r_2^2 + r_3^2) + r_2^4 (r_3^2 + r_1^2) + r_3^4 (r_1^2 + r_2^2) \\
 &\quad + 2r_1^2 r_2^2 r_3^2 - 4L^2 (r_1^2 r_2^2 + r_2^2 r_3^2 + r_3^2 r_1^2)
 \end{aligned} \quad (21)$$

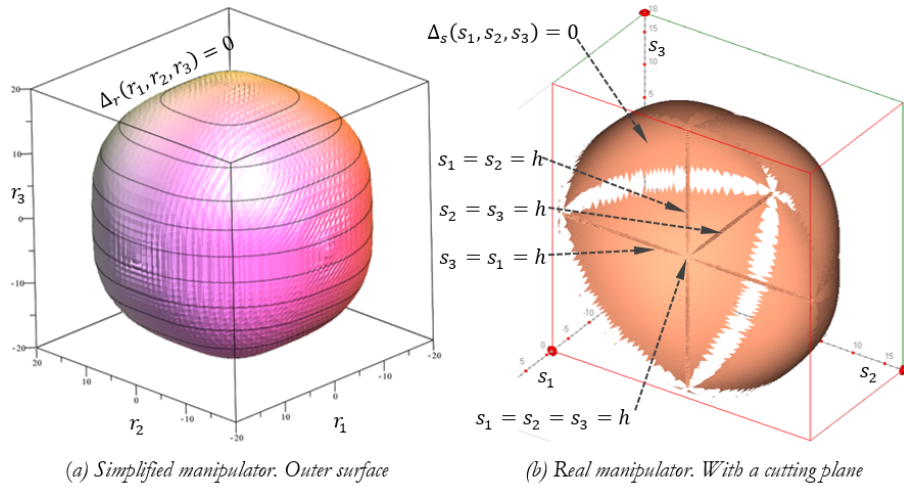


Figure 10. Direct singularity locus in the joint-space

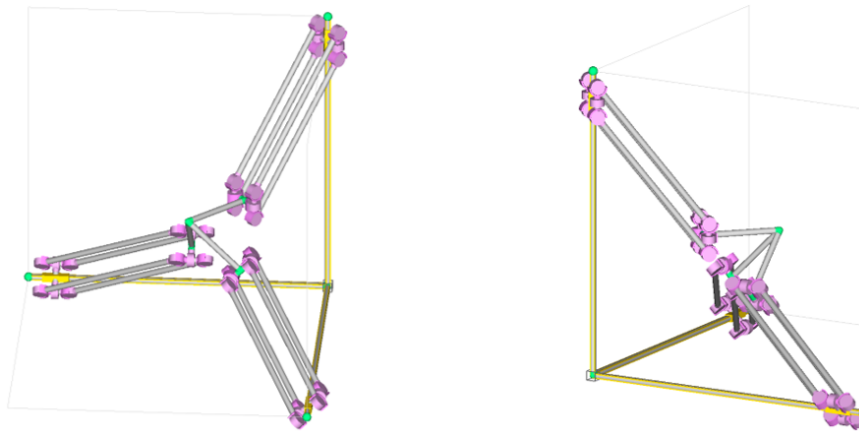


Figure 11. Singular posture. All legs parallel to a plane (two different views).

5 Workspace

To end with the position analysis the workspace of the manipulator is presented. Considering the position equations as they have been obtained, each chain theoretically generates a cylinder parallel to the sliding direction of the prismatic joint. Then, the theoretical workspace would be the intersection of three mutually perpendicular cylinders, as shown in Fig. 8.

Nevertheless, the Pa² joint imposes a limit in the motion range. Since the two parallel Pa cannot lie in the same plane, Fig. 9a, the actual workspace of each chain is just a half cylinder, which produces a smaller real workspace of the whole manipulator, as depicted in Fig. 9b and c.

6 Velocity problem and singularity analysis

To carry out the singularity analysis, the position equations are derived with respect to time and the velocity equations are obtained. The problem is linear in the input and output

velocities, so it can be expressed in a matrix form. In this approach, the Jacobian matrices are obtained. As it can be seen, the rows of the direct Jacobian matrix \mathbf{J}_x are the vectors AB defining the directions of the Pa² joints. The inverse Jacobian matrix \mathbf{J}_q is simpler because it is diagonal. The velocity problem can be expressed as:

$$\mathbf{J}_x \cdot \dot{x} = \mathbf{J}_q \cdot \dot{q}$$

Where:

$$\dot{x} = v_C = \begin{Bmatrix} \dot{x}_C \\ \dot{y}_C \\ \dot{z}_C \end{Bmatrix} \quad \dot{q} = \begin{Bmatrix} \dot{s}_1 \\ \dot{s}_2 \\ \dot{s}_3 \end{Bmatrix} \quad (22)$$

The direct and inverse Jacobian matrices can be obtained from the constraint equations, Eq. (8):

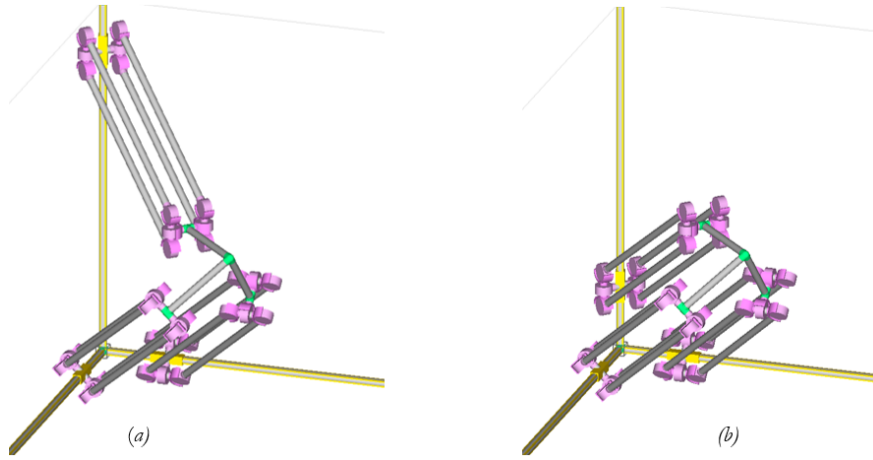


Figure 12. Singular posture. Two and three legs in the same direction

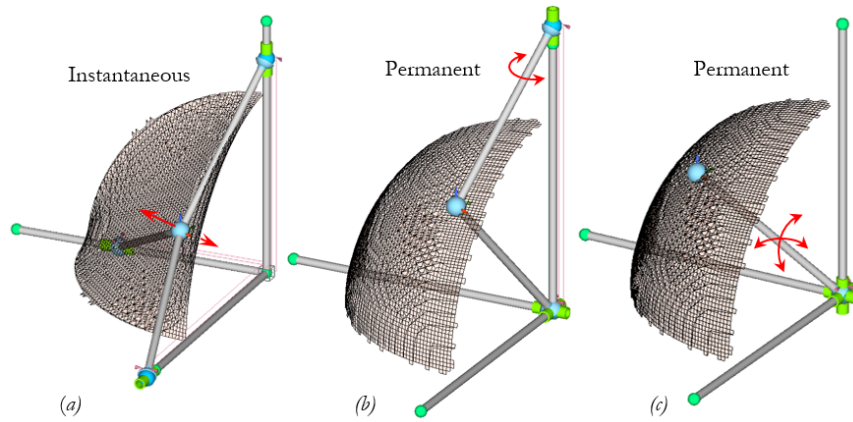


Figure 13. Singular postures in the equivalent manipulator and corresponding singularity surfaces in the workspace.

$$\mathbf{J}_x = \begin{pmatrix} \frac{\partial ec_1}{\partial x_C} & \frac{\partial ec_1}{\partial y_C} & \frac{\partial ec_1}{\partial z_C} \\ \frac{\partial ec_2}{\partial x_C} & \frac{\partial ec_2}{\partial y_C} & \frac{\partial ec_2}{\partial z_C} \\ \frac{\partial ec_3}{\partial x_C} & \frac{\partial ec_3}{\partial y_C} & \frac{\partial ec_3}{\partial z_C} \end{pmatrix}$$

$$\mathbf{J}_q = - \begin{pmatrix} \frac{\partial ec_1}{\partial s_1} & \frac{\partial ec_1}{\partial s_2} & \frac{\partial ec_1}{\partial s_3} \\ \frac{\partial ec_2}{\partial s_1} & \frac{\partial ec_2}{\partial s_2} & \frac{\partial ec_2}{\partial s_3} \\ \frac{\partial ec_3}{\partial s_1} & \frac{\partial ec_3}{\partial s_2} & \frac{\partial ec_3}{\partial s_3} \end{pmatrix} \quad (23)$$

By computing the terms inside \mathbf{J}_x and \mathbf{J}_q , it yields:

$$\begin{pmatrix} x_C - s_1 & y_C - h & z_C - h \\ x_C - h & y_C - s_2 & z_C - h \\ x_C - h & y_C - h & z_C - s_3 \end{pmatrix} \begin{Bmatrix} \dot{x}_C \\ \dot{y}_C \\ \dot{z}_C \end{Bmatrix}$$

$$= - \begin{pmatrix} x_C - s_1 & 0 & 0 \\ 0 & y_C - s_2 & 0 \\ 0 & 0 & z_C - s_3 \end{pmatrix} \begin{Bmatrix} \dot{s}_1 \\ \dot{s}_2 \\ \dot{s}_3 \end{Bmatrix} \quad (24)$$

Direct singularities occur whenever the determinant of the direct Jacobian matrix vanishes. This means that a dependence relation among the input velocities is verified. It is essential to assess these positions because the controllability of the manipulator is lost, so they must be avoided.

The determinant of the direct Jacobian matrix can be obtained as:

$$|\mathbf{J}_x| = x_C s_2 s_3 + y_C s_3 s_1 + z_C s_1 s_2 - s_1 s_2 s_3 - h(x_C s_2 + x_C s_3 + y_C s_3 + y_C s_1 + z_C s_1 + z_C s_2) + h^2(x_C + y_C + z_C + s_1 + s_2 + s_3) - 2h^3 \quad (25)$$

$$\mathbf{J}_x = \begin{pmatrix} x_D - r_1 & y_D & z_D \\ x_D & y_D - r_2 & z_D \\ x_D & y_D & z_D - r_3 \end{pmatrix} \quad (26)$$

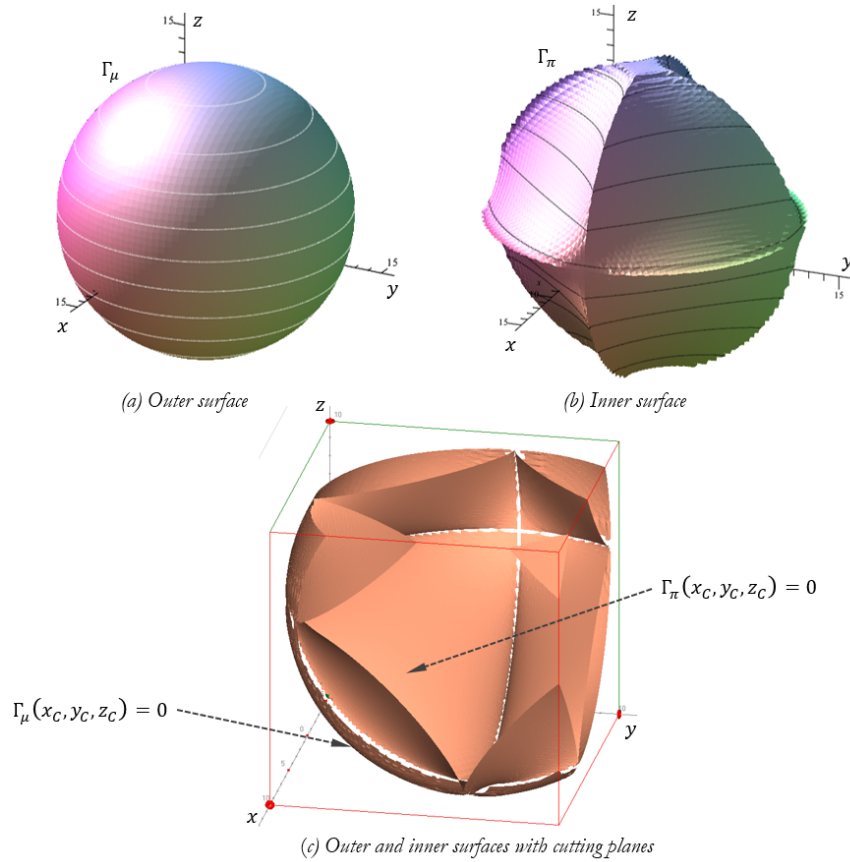


Figure 14. Direct singularity locus in the workspace for the real manipulator.

But the expression is much simpler in the variables of the equivalent manipulator:

$$|\mathbf{J}_x| = x_D r_2 r_3 + y_D r_3 r_1 + z_D r_1 r_2 - r_1 r_2 r_3 \quad (27)$$

Direct singularity surface in the joint-space (input variables domain) is achieved by substituting in the equation $|\mathbf{J}_x| = 0$ the obtained solutions of the direct position problem, Eq. (20). On the one hand, doing this, firstly it is verified that:

$$x_D r_2 r_3 + y_D r_3 r_1 + z_D r_1 r_2 = r_1 r_2 r_3 \pm \sqrt{\Delta_r}/2 \quad (28)$$

So:

$$|\mathbf{J}_x| = 0 \longrightarrow r_1 r_2 r_3 \pm \frac{\sqrt{\Delta_r}}{2} - r_1 r_2 r_3 = 0 \longrightarrow \Delta_r = 0 \quad (29)$$

This first condition, which is a surface in the 3-Dimensional joint space $\Delta_r(r_1, r_2, r_3) = 0$, Eq. (21), can be also expressed in the input variables of the real manipulator $\Delta_s(s_1, s_2, s_3) = 0$, Eq. (14).

On the other hand, apart from the nullity of Δ_r , looking at Eq. (27), it is verified that $|\mathbf{J}_x| = 0$ when any of the following

conditions is satisfied:

$$\begin{cases} r_1 = r_2 = 0 \longrightarrow s_1 = s_2 = h \\ r_2 = r_3 = 0 \longrightarrow s_2 = s_3 = h \\ r_3 = r_1 = 0 \longrightarrow s_3 = s_1 = h \end{cases} \quad (30)$$

These are the expressions of three lines. As it is known, it is verified that direct singularities occur where the mechanism has double solutions of the direct position problem (where the two assembly modes merge). The surface and lines are shown in Fig. 10.

In case of the proposed manipulator, considering the structure of \mathbf{J}_x , along with the mathematical analysis made, a geometrical interpretation is possible. Direct singularities occur when the three chains are parallel to a plane, as shown in Fig. 11, or when two chains have the same direction, as shown in Fig. 12a. Obviously, this second case includes a subcase that occurs when the three legs have the same direction, as depicted in Fig. 12b.

In the singularity locus obtained, the external continuous surface $\Delta_s(s_1, s_2, s_3)$ corresponds to the situation of three legs parallel to a same plane (in the case of the equivalent manipulator, all postures where the three bars lie in the same plane). The three lines correspond to the three possible combinations of two parallel legs. For example, the line

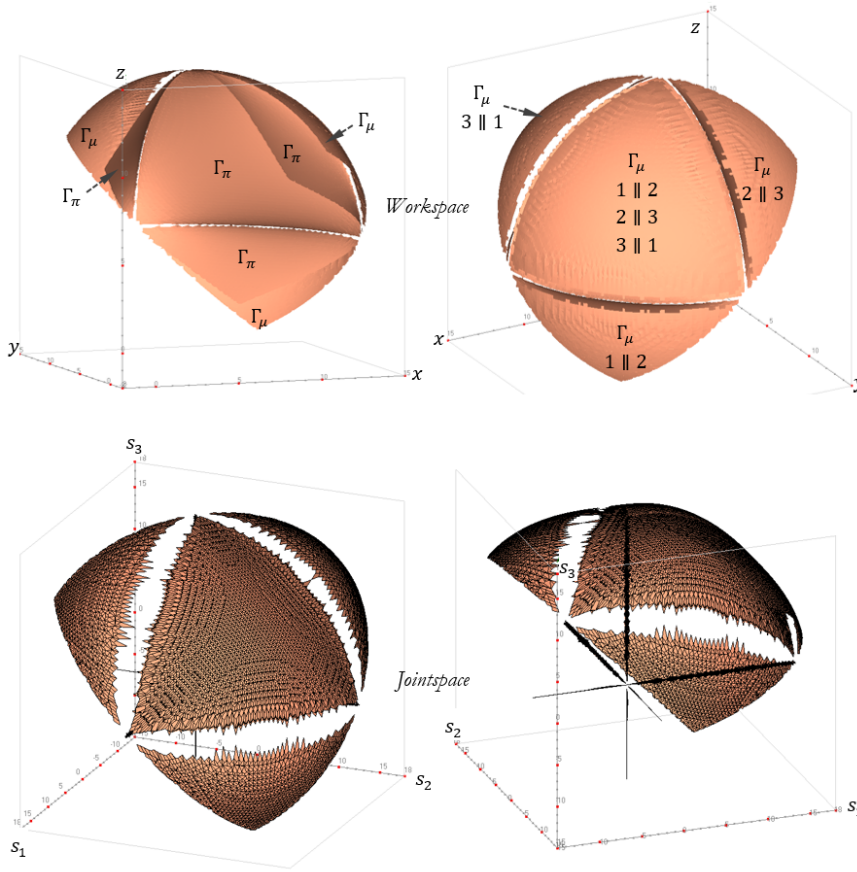


Figure 15. Direct singularity locus in the real workspace and correspondence with the joint-space.

$s_1 = s_2 = h$ corresponds to the case in which the chains 1 and 2 have the same direction. In the case of the equivalent manipulator, this situation ($r_1 = r_2 = 0$) implies that two bars are coincident. The intersection point of the three lines, $s_1 = s_2 = s_3 = h$, corresponds to the subcase of three legs parallel.

Singular postures in the equivalent manipulator are shown next. In the cases of three legs parallel to a same plane, Fig. 13a, or just two legs parallel, Fig. 13b, the rank of \mathbf{J}_x decreases in one (one dof appears with all inputs blocked). In the subcase of the three legs in the same direction, Fig. 13c, the rank of \mathbf{J}_x decreases in two (two dof appear with all inputs blocked).

The direct singularity surface in the workspace (output variables domain) can be also obtained by eliminating input variables from $|\mathbf{J}_x|$:

$$|\mathbf{J}_x| = 0 \longrightarrow \Gamma_\mu(x_D, y_D, z_D) \cdot \Gamma_\pi(x_D, y_D, z_D) = 0 \quad (31)$$

In this case, two independent surfaces, Γ_μ and Γ_π , are obtained. The first surface is:

$$\Gamma_\mu \equiv x_D^2 + y_D^2 + z_D^2 - L^2 = 0 \quad (32)$$

This is a sphere centered at the origin and radius L . The second surface is more complex:

$$\Gamma_\pi \equiv L^{14} - 3L^{12}\sigma + 3L^{10}\sigma^2 - L^8(46\tau + \gamma) + 32L^6\sigma\tau + 8L^4\tau\delta + 80L^2\tau^2 - 16\tau^2\sigma = 0 \quad (33)$$

With:

$$\begin{aligned} \sigma &= x_D^2 + y_D^2 + z_D^2 & \tau &= x_D^2 y_D^2 y_D^2 z_D^2 \\ \gamma &= x_D^6 + y_D^6 + z_D^6 + 3(x_D^4 y_D^2 + x_D^2 y_D^4 + y_D^4 z_D^2 \\ &\quad + y_D^2 z_D^4 + z_D^4 x_D^2 + z_D^2 x_D^4) \\ \delta &= x_D^4 + y_D^4 + z_D^4 + 6(x_D^2 y_D^2 + y_D^2 z_D^2 \\ &\quad + z_D^2 x_D^2) \end{aligned} \quad (34)$$

But once obtained for the simplified equivalent manipulator, both can be easily transformed to the output variables of the real manipulator, $\Gamma_\mu(x_C, y_C, z_C)$, Fig. 14a, and $\Gamma_\pi(x_C, y_C, z_C)$, Fig. 14b. In Fig. 14c both surfaces are represented overlapped and a cross section has been given to visualize the internal part (because Γ_π is inside Γ_μ).

All figures in this and next sections have been obtained for $L = 10$ length units and $h = 5$ length units.

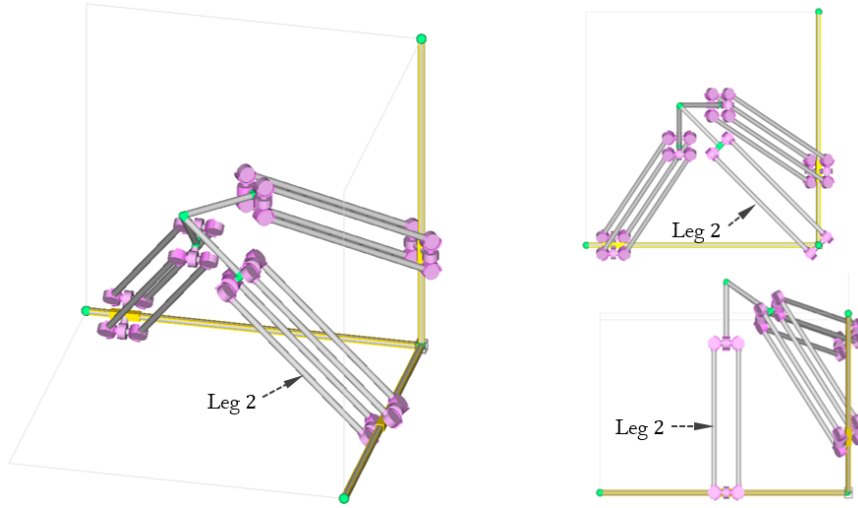


Figure 16. Inverse singular posture.

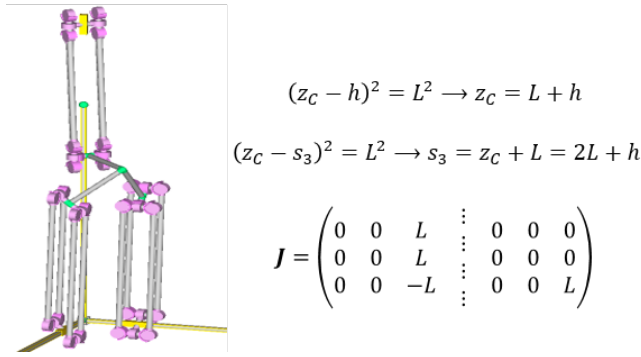


Figure 17. Increased mobility singularity.

In the current domain (output variables), Γ_μ corresponds to the situation where two legs i and j are parallel, $i \parallel j \rightarrow s_i = s_j = h$, and Γ_π where the three legs are parallel to a plane. In addition, Γ_μ is the same surface for the three possible combinations, $s_1 = s_2 = h$, $s_2 = s_3 = h$, and $s_3 = s_1 = h$, and also for the subcase where the three legs have the same direction, $s_1 = s_2 = s_3 = h$. An interesting way to understand how is this possible is to start supposing a posture where the three legs are all of them parallel, and from this position make a working mode change in one chain. Doing this, that leg is not any more parallel to the others, but the remaining two legs are still parallel. This phenomenon is shown in Fig. 12.

Finally, it is possible to depict the direct singularity locus for the real size workspace (that one in Fig. 9, where real motion limits are taken into account) and to obtain also the corresponding actual portions of the theoretical joint-space. In addition, it is possible to identify the specific geometrical conditions associated with each portion as well as the correspondence among the different portions in both domains,

making use of the GIM software as explained in Macho et al. (2009). All this is shown in Fig. 15, where two different views are provided in order to properly show all portions and the existing associations between them.

Inverse singularities occur when the determinant of the inverse Jacobian matrix vanishes. This happens when any chain is in a completely extended position, that is, inverse singularities define the workspace boundaries. Taking into account that:

$$\mathbf{J}_q = \begin{pmatrix} x_C - s_1 & 0 & 0 \\ 0 & y_C - s_2 & 0 \\ 0 & 0 & z_C - s_3 \end{pmatrix} = \begin{pmatrix} x_D - r_1 & 0 & 0 \\ 0 & y_D - r_2 & 0 \\ 0 & 0 & z_D - r_3 \end{pmatrix} \quad (35)$$

Then:

$$|\mathbf{J}_q| = (x_C - s_1)(y_C - s_2)(z_C - s_3) = (x_D - r_1)(y_D - r_2)(z_D - r_3) \quad (36)$$

So:

$$|\mathbf{J}_q| = 0 \rightarrow \begin{cases} x_C = s_1 \rightarrow (y_C - h)^2 + (z_C - h)^2 = L^2 \\ y_C = s_2 \rightarrow (x_C - h)^2 + (z_C - h)^2 = L^2 \\ z_C = s_3 \rightarrow (x_C - h)^2 + (y_C - h)^2 = L^2 \end{cases} \rightarrow \begin{cases} x_D = r_1 \rightarrow y_D^2 + z_D^2 = L^2 \\ y_D = r_2 \rightarrow x_D^2 + z_D^2 = L^2 \\ z_D = r_3 \rightarrow x_D^2 + y_D^2 = L^2 \end{cases} \quad (37)$$

These are the same surfaces depicted in Fig. 8. In Fig. 16 is shown the case of leg 2 totally extended, that is, a posture where the working modes $\otimes p \otimes$ and $\otimes n \otimes$ meet (where \otimes means p or n).

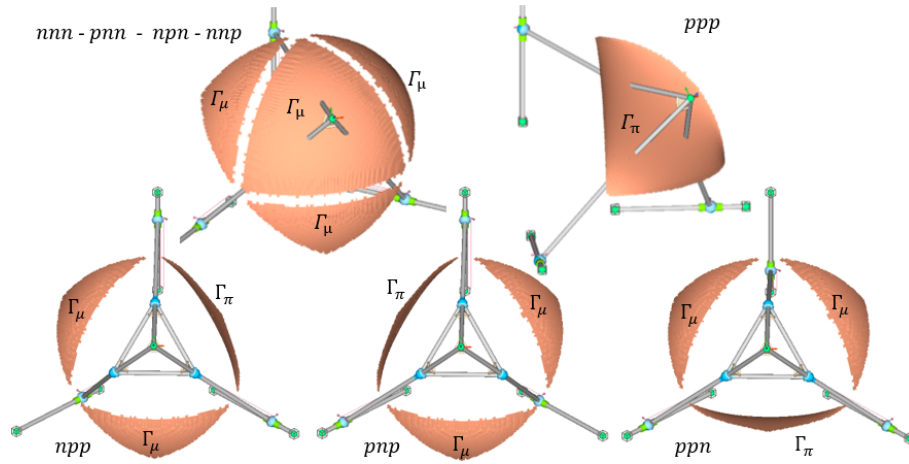


Figure 18. Specific direct singularities for the different working modes in the workspace.

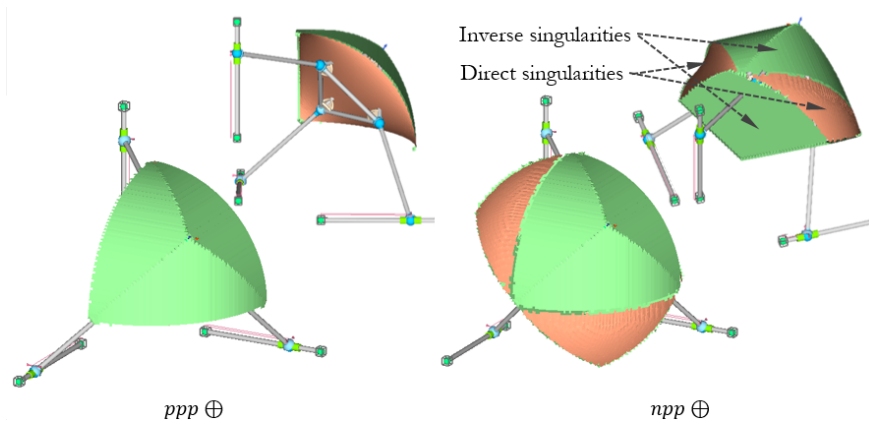


Figure 19. Singularity-free regions for two of the eight working modes (two different views for each one).

Increased mobility singularities occur when the complete Jacobian matrix is rank deficient. The complete Jacobian is defined as:

$$\mathbf{J} \begin{Bmatrix} \dot{x} \\ \dot{q} \end{Bmatrix} = 0 \longrightarrow J = \left(\mathbf{J}_x \quad \vdots \quad -\mathbf{J}_q \right) \quad (38)$$

So, for the manipulator under study:

$$\mathbf{J} = \begin{pmatrix} x_C - s_1 & y_C - h & z_C - h & \vdots & -(x_C - s_1) & 0 & 0 \\ x_C - h & y_C - s_2 & z_C - h & \vdots & 0 & -(y_C - s_2) & 0 \\ x_C - h & y_C - h & z_C - s_3 & \vdots & 0 & 0 & -(z_C - s_3) \end{pmatrix} \quad (39)$$

Now, the specific conditions to verify the rank deficiency can be found. Here it will be shown an example. Firstly, note that when two legs are parallel, the locus of coupler point positions is a sphere centered at (h, h, h) and radius L . For legs 1 and 2 being parallel, $s_1 = s_2 = h$. Over this surface, defined in the three output variables, the values of two variables can be freely chosen. So, it is possible to set the posture where

$x_C = y_C = h$. For these values, from the positions equations, Eq. (8), are obtained the values of z_C and s_3 . Then, the posture of the manipulator, as well as the Jacobian matrix are shown in Fig. 17. It is obvious that the rank of this matrix decreases from 3 to 2.

7 Operational workspace

The direct singularity locus for the real size workspace was depicted in Fig. 15. This surface comprises all existing working modes and this means that it cannot be directly used as it has been obtained. The problem is that each point of such a surface, which corresponds to a position of the coupler point C , is, in fact, compatible with as many different postures of the manipulator as existing working modes, but just one of those working modes will be in a real direct singularity. In other words, each working mode has its specific direct singularities, and the singularity locus that has been obtained analytically is the overlap of all of them.

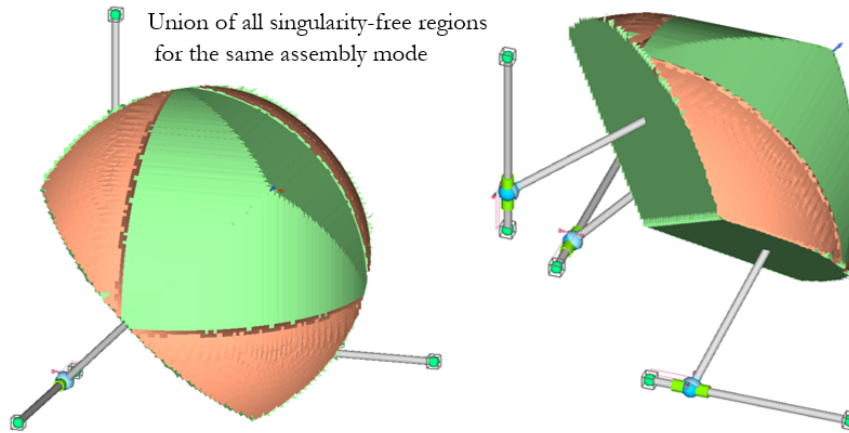


Figure 20. Enlarged operational workspace for assembly mode \oplus (two different views).

Then, it is necessary to identify the portions of the singularity surface that are specifically associated with each working mode, that is, it is necessary to distribute the whole singularity locus among the eight existing working modes, evaluating the value of $|J_q|$ at each point of the singularity surface for all existing working modes, as explained in Salgado et al. (2008). The result of this process is shown in Fig. 18, where in order to gain clarity, instead of the real manipulator, the schematic kinematic chains have been represented. The common situation for a parallel manipulator is having different singularities for each working mode, but in this case, due to the phenomenon previously described (the singularity surface when three or two legs are parallel is the same) there are four working modes sharing the same singularities.

Now, once the specific direct singularities of each working mode have been identified, the singularity-free regions in the workspace can be traced. For each working mode, the theoretical workspace is completely crossed by the singular surface and is divided into adjacent regions associated with the existing assembly modes. Both assembly modes can be identified as \oplus and \ominus because each one is associated with one sign of $|\mathbf{J}_x|$ (and separated by positions where $|\mathbf{J}_x| = 0$). For each working mode, these singularity-free regions are considered the operational workspaces. In Fig. 19, the safe regions for two working modes (ppp and npp) are shown, both for a same assembly mode (\oplus).

Although inverse singularities are positions where the platform mobility is restrained, because a dependence relation among output velocities is satisfied, they are not a problem from the actuators control point of view. They can be reached during the motion and, in fact, communicate the regions associated with the different working modes (for the same assembly mode), so they can be used to enlarge the operational workspace. When a workspace boundary (where two solutions of the inverse position problem merge) is reached, the manipulator can change its working mode and make a transi-

tion from one workspace region to another, maintaining the same assembly mode, Macho et al. (2008, 2009, 2013).

Taking advantage of the possibility of carrying out this type of transitions, all regions associated with the same assembly mode, for all working modes, can be communicated and therefore the operational workspace can be enlarged. In Fig. 20 is shown the enlarged operational workspaces associated with one of the two existing assembly modes.

8 Conclusions

In this paper, the potentiality of the use of the Pa² pair as an adequate kinematic chain to design translational parallel manipulators is studied. After a deep kinematic analysis, it is stated that the position and velocity equations are simpler than those of chains based on revolute joints to obtain translational motion patterns. Additionally, the architecture based on the Pa² pair, is more robust than the designs based on two consecutive floating prismatic joints avoiding the problems of galling and blocking that can appear in the passive prismatic joints. Also, the Pa² pair includes a structure based on four parallel bars structure that provides the manipulator with high stiffness and accuracy.

From a practical approach, the Pa² pair is used in the design of a 3 – PPa² translational parallel manipulator which is completely kinematically characterized by the solving of the position and velocity problem, the singularity analysis and the workspace computation. The results are obtained in terms of simplicity of the architecture and the position and velocity equations. The possibility of enlarging the operational workspace confirms the interest of the proposed manipulator design implementing the studied Pa² pairs.

Given the potentiality of this manipulator, the design of 3 – PPa² could be enhanced regarding the dimensional synthesis and optimization process, with the purpose of developing a real prototype in which also constructive considerations, reliability, stiffness and easiness of assembly should

be considered. Additionally, by studying the possibilities of eliminating redundant constraints of the Pa² pair, non-redundant designs could be synthesized to reduce as much as possible the influence of the manufacturing tolerances in the kinematic and dynamic behavior of the translational manipulator.

Code availability. All the figures in the paper have been obtained using GIM software (www.ehu.eus/compmech/software) with the exception of Figs. 10 and 14 that have been obtained using commercial mathematical software (MAPLE).

Competing interests. The authors declare that they have no conflict of interest.

Acknowledgements. This study was funded by the Spanish Government through the *Ministerio de Economía y Competitividad* (Project DPI2015-67626-P, MINECO/FEDER, UE), the financial support from the *University of the Basque Country* (UPV/EHU) under the program UFI 11/29 and the support to the research group, through the project with ref. IT949-16, given by the *Departamento de Educación, Política Lingüística y Cultura* of the Regional Government of the Basque Country.

Edited by: Andreas Müller

Reviewed by: two anonymous referees

References

- Affi, Z., Romdhane, L., and Maalej, A.: Dimensional synthesis of a 3-translational-DOF in-parallel manipulator for a desired workspace, *Eur. J. Mech. A-Solid.*, 23, 311–324, 2004.
- Angeles, J.: The qualitative synthesis of parallel manipulators, *ASME Journal of Mechanical Design*, 126, 617–624, 2004.
- Angeles, J.: The degree of freedom of parallel robots: a Group-Theoretic approach, *IEEE Int. Conf. Robot.*, Barcelona, Spain, 2005.
- Arai, T., Hervé, J. M., and Tanikawa, T.: Development of 3 DOF Micro Finger, *Proc. IROS'96*, 5–8 November, Osaka, 981–987, 1996.
- Ceccarelli, M. and Ottaviano, E.: An analytical design for CaPaMan with prescribed position and orientation, in: 2000 ASME Biennial Mechanisms and Robotics Conference, Baltimore, Maryland, paper DETC2000/MECH-14099, 2000.
- Clavel, R.: Delta, a fast robot with parallel geometry, *Proc. 18th Int. Symp. Industrial Robots*, Lausanne, Switzerland, 91–100, 1988.
- Gogú, G.: Structural synthesis of fully-isotropic translational parallel robots via theory of linear transformations, *Eur. J. Mech. A-Solid.*, 23, 1021–1039, 2004.
- Hernandez, A., Zhang, Z., Petuya, V., Macho, E., and Amezuza, E.: Translational Parallel Manipulator with Pa² Kinematic Joints, *The Joint International Conference of the XII International Conference on Mechanisms and Mechanical Transmissions and the XXIII International Conference on Robotics (MTM & Robotics 2016)*, 26–27 October, Aachen, Germany, 2016a.
- Hernandez, A., Zhang, Z., Petuya, V., Macho, E., and Amezuza, E.: Manipuladores paralelos de traslación con pares Pa², *XXI Congreso Nacional de Ingeniería Mecánica – CNIM 2016*, 9–11 October, Elche, Spain, 2016b.
- Hervé, J. M.: The Lie group of rigid body displacements, a fundamental tool for mechanism design, *Mech. Mach. Theory*, 34, 719–730, 1999.
- Hervé, J. M. and Sparacino, F.: Star, a new concept in robotics, *Proc. 3rd Int. Workshop on Advances in Robot Kinematics*, 7–9 September, Ferrara, 176–183, 1992.
- Huang, T., Li, Z., Li, M., Chetwynd, D. G., and Gosselin, C. M.: Conceptual Design and Dimensional Synthesis of a Novel 2-DOF Translational Parallel Robot for Pick-and-Place Operations, *J. Mech. Design*, 126, 449–455, 2004.
- Li, Z., Lou, Y., Zhang, Y., Liao, B., and Li, Z.: Type Synthesis, Kinematic Analysis, and Optimal Design of a Novel Class of Schönflies-Motion Parallel Manipulators, *IEEE T. Autom. Sci. Eng.*, 10, 674–686, 2013.
- Macho, E., Altuzarra, O., Pinto, C., and Hernández, A.: Workspaces associated to assembly modes of the 5R planar parallel manipulator, *Robotica*, 26, 395–403, 2008.
- Macho, E., Altuzarra, O., Amezuza, E., and Hernández, A.: Obtaining configuration space and singularity maps for parallel manipulators, *Mech. Mach. Theory*, 44, 2110–2125, 2009.
- Macho, E., Altuzarra, O., Pinto, C., and Hernández, A.: Enlarging operational workspaces in parallel manipulators by connecting working mode spaces. Application to the 3RSS robot, *Robotica*, 31, 539–548, 2013.
- Pierrot, F. and Company, O.: H4: A new family of 4-dof parallel robots, *Proc. AIM 1999: IEEE/ASME Int. Conf. Adv. Intell. Mechatron.*, Atlanta, GA, 508–513, 1999.
- Pierrot, F., Nabat, V., Company, O., Krut, S., and Poignet, P.: Optimal Design of a 4-DOF Parallel Manipulator: From Academia to Industry, *IEEE T. Robot.*, 25, 213–224, 2009.
- Salgado, O.: Síntesis, Análisis y Diseño de Manipuladores Paralelos de Baja Movilidad, *Doctoral Thesis, Faculty of Engineering in Bilbao, University of the Basque Country (UPV/EHU)*, 2008 (in Spanish).
- Salgado, O., Altuzarra, O., Amezuza, E., and Hernández, A.: A Parallelogram-Based Parallel Manipulator for Schönflies Motion, *Journal of Mechanical Design*, 129, 1243–1250, 2007.
- Salgado, O., Altuzarra, O., Petuya, V., and Hernández, A.: Synthesis and Design of a Novel 3T1R Fully-Parallel Manipulator, *J. Mech. Design*, 130, 042305-1–042305-8, <https://doi.org/10.1115/1.2839005>, 2008.
- Yu, J., Dai, J. S., Zhao, T., Bi, S., and Zong, G.: Mobility analysis of complex joints by means of screw Theory, *Robotica*, 27, 915–927, 2009.